



Parameterization and
global implications

G. S. Stuart et al.

This discussion paper is/has been under review for the journal Atmospheric Chemistry and Physics (ACP). Please refer to the corresponding final paper in ACP if available.

Reduced efficacy of marine cloud brightening geoengineering due to in-plume aerosol coagulation: parameterization and global implications

G. S. Stuart¹, R. G. Stevens¹, A.-I. Partanen³, A. K. L. Jenkins², H. Korhonen³, P. M. Forster², D. V. Spracklen², and J. R. Pierce^{1,4}

¹Physics and Atmospheric Science, Dalhousie University, Halifax, NS, Canada

²School of Earth and Environment, University of Leeds, Leeds, UK

³Kuopio Unit, Finnish Meteorological Institute, Kuopio, Finland

⁴Department of Atmospheric Science, Colorado State University, Fort Collins, CO, USA

Received: 7 June 2013 – Accepted: 19 June 2013 – Published: 12 July 2013

Correspondence to: R. G. Stevens (rgstevens@dal.ca)

Published by Copernicus Publications on behalf of the European Geosciences Union.

Title Page

Abstract

Introduction

Conclusions

References

Tables

Figures

◀

▶

◀

▶

Back

Close

Full Screen / Esc

Printer-friendly Version

Interactive Discussion



Abstract

The intentional enhancement of cloud albedo via controlled sea-spray injection from ships (Marine Cloud Brightening) has been proposed as a possible method to control anthropogenic global warming; however, there remains significant uncertainty in the efficacy of this method due to, amongst other factors, uncertainties in aerosol and cloud microphysics. A major assumption used in recent cloud- and climate-modeling studies is that all sea spray was emitted uniformly into some oceanic grid boxes, and thus these studies did not account for sub-grid aerosol coagulation within the sea-spray plumes. We explore the evolution of these sea-salt plumes using a multi-shelled Gaussian plume model with size-resolved aerosol coagulation. We determine how the final number of particles depends on meteorological conditions, including wind speed and boundary-layer stability, as well as the emission rate and size distribution of aerosol emitted. Under previously proposed injection rates and typical marine conditions, we find that the number of aerosol particles is reduced by over 50 %, but this reduction varies from under 10 % to over 90 % depending on the conditions. We provide a computationally efficient parameterization for cloud-resolving and global-scale models to account for sub-grid scale coagulation, and we implement this parameterization in a global-scale aerosol-climate model. We find that accounting for this sub-grid scale coagulation reduces cloud droplet number concentrations by 46 % over emission regions, and reduces the global mean radiative flux perturbation from -1.5 W m^{-2} to -0.8 W m^{-2} .

1 Introduction

Anthropogenic greenhouse-gas emissions rates are increasing (Forster et al., 2007), and it appears to be unlikely that drastic reductions in these rates will take place in the near future (Rosa and Deitz, 2012). Geoengineering, the deliberate manipulation of the Earth's climate, provides possible but imperfect methods of slowing the global

ACPD

13, 18679–18711, 2013

Parameterization and global implications

G. S. Stuart et al.

Title Page

Abstract

Introduction

Conclusions

References

Tables

Figures

◀

▶

◀

▶

Back

Close

Full Screen / Esc

Printer-friendly Version

Interactive Discussion



**Parameterization and
global implications**

G. S. Stuart et al.

Title Page

Abstract

Introduction

Conclusions

References

Tables

Figures

◀

▶

◀

▶

Back

Close

Full Screen / Esc

Printer-friendly Version

Interactive Discussion



the square of particle concentrations, coagulation will occur most quickly in the initial, dense plume. This coagulation may be important in reducing the number of potential CCN that reach the cloud and has not yet been treated in models. Thus, the efficacy of prior estimates of sea-salt geoengineering may have been over-predicted due to the lack of these in-plume coagulation effects.

We explore the evolution of the sea-salt size distribution in these emissions plumes using a multi-shelled Gaussian plume model with size-resolved aerosol coagulation. The influence of the emissions rate and the emitted size distribution as well as local atmospheric conditions (wind speed and boundary-layer stability) and the stack radius on the final number and size of particles is determined using this model. We use the results of the plume model to create a computationally efficient parameterization of the loss of particle number by coagulation in plumes for cloud-resolving and global models. We then implement the parameterization in a global-scale aerosol-climate model, and show the effect on predictions of marine cloud brightening efficacy.

We describe the Gaussian-plume model used for this study, a high-resolution large-eddy simulation model used for evaluation of the Gaussian-plume model, and the global model in Sect. 2. The case descriptions are shown in Sect. 3. We introduce the form of the parameterization in Sect. 4. We evaluate the parameterization and show the sensitivities to each variable in Sect. 5. We describe the global model experimental design and show the global model results in Sect. 6. Finally, we present our conclusions in Sect. 7.

2 Model descriptions

2.1 Gaussian-plume model

We use a multi-shelled Gaussian plume model to assess the effects of coagulation on the sea spray particle size distribution (Fig. 1). The design of the model follows Lazaridis et al. (2001). The model follows the mean wind speed as a Lagrangian parcel,

**Parameterization and
global implications**

G. S. Stuart et al.

Title Page

Abstract

Introduction

Conclusions

References

Tables

Figures

◀

▶

◀

▶

Back

Close

Full Screen / Esc

Printer-friendly Version

Interactive Discussion



and the 10 shells expand with distance from the source following the expansion of a Gaussian plume (Seinfeld and Pandis, 2006). The outsides of the 10 shells represent 0.3, 0.6, 0.9, 1.2, 1.5, 1.8, 2.1, 2.4, 2.7 and 3.0 standard deviations of the particle number concentration across the Gaussian plume. The expansion of the shells with distance uses the method of Klug (1969) with the plume expanding more quickly under unstable conditions than stable conditions (stability classes discussed in Sect. 3). The initial 1-standard-deviation plume width is set equal to the diameter of the emissions stack (2.4 m as a base-case approximation but varied later). The depth of the shells (in the direction of the wind) is set arbitrarily to 10 m. We assume that coagulation occurs through Brownian coagulation only, and we calculate the coagulation kernel using the method of Fuchs (1964). Similar plume models have shown good agreement with field measurements downwind from power plants (Hudischewsky and Seigneur, 1989; Lazaridis et al., 2001), and have been used to predict plume visibility (Seigneur et al., 1997) and to study mercury speciation, transport and deposition (Lohman et al., 2006).

The model tracks the aerosol size distribution using 100 size bins, spaced logarithmically between 10 nm and 10 μ m in wet diameter (at 80 % relative humidity, RH). Particles are added to the plume at the beginning of the simulation corresponding to the number of particles that would be emitted into a 10 m-deep box (and the width of the stack diameter) if the box is traveling at the same speed as the wind. The higher particle concentrations near the center of the plume cause faster coagulation near the center and thus a difference in the shape of the size distribution between the center and outside of the plume. While inert species do not need to be transferred between the shells of the plume (the expansion of the shells accounts for diffusion), this enhanced coagulation near the middle of the plume requires us to account for a net diffusion of big particles from the center shells outward and a net diffusion of smaller particles from outer shells inward (Fig. 1). To calculate the rate of this net diffusion between shells, we normalize the size-dependent aerosol concentrations by an inert tracer (which allows us to determine if coagulation has caused an increase or decrease in the number of

aerosols in the size bin) and then calculate the diffusion of the normalized values using Fick's Law. The model uses a varying time-step to speed up calculation during periods of low coagulation.

We represent the emitted aerosols using a single lognormal mode or a single monodisperse size. We vary the number-median diameter and the width of the mode to determine the effect on the fraction of particles remaining after in-plume coagulation. We represent the background marine aerosol using the two-mode lognormal distribution as described in Heintzenburg et al. (2000). However, we find that these background particles have a negligible effect on the results because the concentrations are small compared to the concentrations of emitted sea spray. Increasing the background concentrations by a factor of 10 decreased the number of remaining emitted particles by less than 0.001 % under the base-case emissions conditions described shortly.

Condensable sulfate and organic vapors are not currently included in the model. The concentrations of sea-spray aerosols in these plumes will be sufficiently large compared to the concentrations of secondary vapors during the short time that is being simulated that the effects of condensation on the aerosol size distributions will be insignificant.

Our model has several limitations. We assume that the wet aerosol and the air reach an instant equilibrium at 80 % RH. There are two implications of this: (1) the size of the particles may be different than we assume (however, we do show later that the results are less sensitive to size than other factors), and (2) the evaporation of the droplets may affect the dynamics of the plume (e.g. the plume is cooler than its surroundings and sinks) and affect the mixing rate of the plume. We assume that our plume is perfectly Gaussian. Turbulent plumes in unstable boundary layers are only Gaussian when time-averaged. An actual plume may have higher- and lower-concentration regions, and because of the quadratic relationship of the rate of coagulation with concentrations, this could cause our model to slightly under-predict coagulation in unstable boundary layers (Stevens et al., 2012). We assume that the plume can expand without bounds. An actual plume will be limited in the vertical direction by the ocean surface below and

Parameterization and global implications

G. S. Stuart et al.

[Title Page](#)[Abstract](#)[Introduction](#)[Conclusions](#)[References](#)[Tables](#)[Figures](#)[◀](#)[▶](#)[◀](#)[▶](#)[Back](#)[Close](#)[Full Screen / Esc](#)[Printer-friendly Version](#)[Interactive Discussion](#)

**Parameterization and
global implications**

G. S. Stuart et al.

Title Page

Abstract

Introduction

Conclusions

References

Tables

Figures

◀

▶

◀

▶

Back

Close

Full Screen / Esc

Printer-friendly Version

Interactive Discussion



lation was carried out for 88 model seconds. Simulations with this model suggest that despite the relatively coarse resolution for representing the ~ 2.5 m outlet diameter, this model configuration successfully reproduces key dynamical features that are characteristic of an emission jet into a crosswind flow (Mahesh, 2013), including a counter-rotating vortex pair. The particles were preferentially distributed at the center of the vortex pair, also as expected (Tu and Liu, 2012; Wen et al., 1992). The high-resolution LES model therefore can resolve fluid-dynamics features that cannot be resolved by a Gaussian-plume model. We compare the results of the LES model with those of the Gaussian-plume model in Sect. 5.

2.3 Global-scale aerosol-climate model

For the global simulations to evaluate the effect of the parameterization, we used aerosol-climate model ECHAM-HAMMOZ (ECHAM5.5-HAM2) (Stier et al., 2005; Zhang et al., 2012) with the same model and experiment setup as in geoengineering simulations described by Partanen et al. (2012). The aerosol microphysics module M7 (Vignati et al., 2004) describes internally and externally mixed aerosol distribution with seven log-normal modes consisting of sulfate, sea salt, organic carbon, black carbon and mineral dust. The model calculates nucleation of new particles, condensation of sulfuric acid vapor, coagulation, uptake of water, and removal of aerosols by dry deposition, sedimentation, and wet deposition.

Aerosol emissions from anthropogenic sources and biomass burning were taken from the AEROCOM data base (Dentener et al., 2006) for the year 2000. Dust, dimethyl sulfide, and natural sea salt emissions were calculated online as described by Zhang et al. (2012).

The cloud droplet activation was calculated online with a physically based parameterization (Abdul-Razzak and Ghan, 2000; Lohmann et al., 2007). Updraft velocity in stratiform clouds for the activation parameterization was calculated as the sum of grid-mean vertical velocity and a turbulent contribution (Lohmann and Hoose, 2009). Cloud microphysics (including both first and second indirect effects) were calculated as de-

scribed by Lohmann and Hoose (2009). The combination of the model version and the cloud activation parameterization is unpublished and may differ from the official model version to be released with respect to e.g. model tuning parameters.

3 Gaussian-plume model case descriptions

In this study, we test the sensitivity of the “fraction of particles remaining” (the final particle number divided by the initial particle number) to the wind speed (v_w), particle number emissions rate (P), the emissions number-median dry diameter (D_p), the emissions geometric standard deviation (σ) and the emission-source radius (R_s). The maximum, minimum and base-case values are provided in Table 1. Our base case uses particle emissions with a D_p of 200 nm, which correspond to the size of a dry sea-spray particle obtained from an 800 nm seawater drop (Lewis and Schwartz, 2004) as described in Salter (2008). The emitted σ is set arbitrarily to 1.2 in the base case. Salter (2008) describes sea-spray emissions at a total sea-water flow rate of 30 kg s^{-1} . This flow rate, if broken up into the 200-nm dry diameter (800-nm wet diameter) mode described above, corresponds to an aerosol number emissions rate of $1.1 \times 10^{17} \text{ s}^{-1}$, which we use as our base-case value for P . We use a base-case v_w of 8 m s^{-1} , which corresponds to the minimum wind speed needed to obtain a sea-water flow rate of 30 kg s^{-1} as described in Salter (2008) and Korhonen et al. (2010). The minimum and maximum values in Table 1 allow us to both test the sensitivity of the fraction of particles remaining to each of the five parameters as well as allow us to create a parameterization of the fraction of particles remaining for large-scale models.

Additionally, we evaluate the fraction of particles remaining under the six Pasquill stability classes (Pasquill, 1961): A, extremely unstable; B, moderately unstable; C, slightly unstable; D, neutral; E, slightly stable; and F, moderately stable. Because the marine boundary layer is often close to neutral stability, our base stability is D; however, we test all conditions and build the parameterization for each.

Title Page

Abstract

Introduction

Conclusions

References

Tables

Figures

◀

▶

◀

▶

Back

Close

Full Screen / Esc

Printer-friendly Version

Interactive Discussion



4 Parameterization formulation

Using the Gaussian-plume model described above, we have created a computationally efficient parameterization of the loss of particle number by coagulation in plumes for use in cloud-resolving and global models. In this section we introduce the form of the parameterization.

Turco and Yu (1997) give analytic solutions for the change in number due to coagulation for expanding plumes. They give the number of particles N_p that is asymptotically reached with time as:

$$N_p = \frac{N_{po} N_T}{N_{po} + N_T} \quad (1)$$

Where N_{po} is the initial number of particles, and N_T is defined for plumes that expand super-linearly with time as:

$$N_T = \frac{2V_o(\alpha - 1)}{K_c t_i} \quad (2)$$

Where V_o is the initial volume, t_i is the time it would take the plume to expand from a point source to its initial volume given its rate of expansion, K_c is the effective coagulation kernel, and α is a parameter that dictates the rate of expansion, which is a function of the atmospheric stability. If we define F as the fraction of particles remaining (N_p/N_{po}), we can rearrange Eq. (1) and substitute Eq. (2) to give:

$$F = \frac{2V_o(\alpha - 1)}{K_c t_i N_{po} + 2V_o(\alpha - 1)} \quad (3)$$

To simplify this further, we can divide through by V_o to get:

$$F = \frac{2(\alpha - 1)}{K_c t_i C_o + 2(\alpha - 1)} \quad (4)$$

Title Page

Abstract

Introduction

Conclusions

References

Tables

Figures

◀

▶

◀

▶

Back

Close

Full Screen / Esc

Printer-friendly Version

Interactive Discussion



Where C_o is the initial particle concentration.

Our goal is to fit F to five different parameters: wind speed (v_w), emission stack radius (R_s), particle emission rate (P), particle mean-diameter (D_p), and the geometric standard deviation of the size distribution (σ). We note that α depends only on the boundary-layer stability, and that we can incorporate $2(\alpha - 1)$ into a constant dependent only upon the stability class. The other factors must only affect the $K_c t_i C_o$ term. We therefore choose to fit our multi-shelled Gaussian plume model data to a semi-empirical equation of the form:

$$F = \frac{k}{\left(\frac{v_w}{v_{w0}}\right)^a \left(\frac{R_s}{R_{s0}}\right)^b \left(\frac{P}{P_0}\right)^c \left(\frac{\sigma}{\sigma_0}\right)^d \left(\frac{D_p}{D_{p0}}\right)^e + k} \quad (5)$$

where the constants “ a ” through “ e ” along with k are fitted parameters for each stability class, and the “ $_0$ ” subscripts denote the base case conditions (Table 1). Thus, the fraction of the particles remaining would be a function of the five parameters and the stability class, which may be provided by a cloud-resolving or global model. As Supplement, we provide Fortran code of this parameterization for use in these models.

To sample the entire parameter space to create training data for the fit of the parameterization, we have used a pseudo-random Latin hypercube (McKay, 1979) in order to choose our parameters for 1000 simulations of the multi-shelled Gaussian-plume model for each boundary-layer stability. A Latin hypercube is a method of sampling a parameter space such that the full range of each parameter is sampled evenly, but the values of each variable are uncorrelated. Using a least-squares fitting, we calculated the best-fit values of a, b, c, d, e and k for the parameterization, and these values, as well as goodness-of-fit metrics, are shown in Table 2. We will discuss the best-fit values and the parameterization results in the following section.

Parameterization and
global implications

G. S. Stuart et al.

Title Page

Abstract

Introduction

Conclusions

References

Tables

Figures

◀

▶

◀

▶

Back

Close

Full Screen / Esc

Printer-friendly Version

Interactive Discussion



5 Gaussian-plume model results

As a demonstration of the coagulation within the multiple shells of the model, Fig. 2 shows the fraction of particles remaining and particle concentrations for 18 000 s (5 h) for the base case. We show the values for each shell as well as the plume scale averages. We also show the results of a high-resolution large eddy simulation (LES) model for comparison, described in Sect. 2.2. The LES model results will be discussed in the following paragraph. Particle concentrations are affected by both coagulation and plume expansion while the fraction of particles remaining is affected only by coagulation. As would be expected, the inner-most shells with the highest initial particle concentrations show the largest fractional loss in particle number due to coagulation. Figure 2 shows that over 80 % of coagulation occurs in the first 10 s, which would correspond to plume spatial scales (about 10 m wide by 4 m tall for neutral stability) and distances downwind (80 m) that are smaller than the resolution of most cloud models. Coagulation slows and the fraction of particles remaining reaches an asymptote after about 300 s (5 min). For all future simulations in this paper, we simulate 3000 s (50 min), which will include the majority of the coagulation under all conditions. Additionally for the remainder of the paper, we will only present the overall fraction of particles remaining across all shells as this overall fraction is what is most useful for cloud and global models.

In order to evaluate the presented Gaussian plume model results, we also show the results of a high-resolution LES model, described in Sect. 2.2. We note that the values of the wind speed used in the LES model, are similar, but not equal, to those used as the base case for the Gaussian-plume model, and that the aerosols are emitted at a single monodisperse size, where they were emitted as a lognormal mode in the Gaussian-plume model simulations in Fig. 2. Additionally, the Gaussian-plume model simulations do not have an initial upwards velocity. In spite of the very different approach of this LES modeling technique to the Gaussian plume model, and slight disparities in initial conditions, the time series of fraction of particles remaining (Fig. 2a)

Parameterization and global implications

G. S. Stuart et al.

[Title Page](#)[Abstract](#)[Introduction](#)[Conclusions](#)[References](#)[Tables](#)[Figures](#)[◀](#)[▶](#)[◀](#)[▶](#)[Back](#)[Close](#)[Full Screen / Esc](#)[Printer-friendly Version](#)[Interactive Discussion](#)

show notable similarities, particularly in asymptotic behavior and limits, which gives us confidence in the results of the multi-shelled Gaussian plume model.

As discussed in Sect. 4, we used least-squares fitting to calculate the best-fit values of the exponents and the constant for the parameterization (Eq. 5) for each stability class. The exponents for the wind speed, “ a ”, and for the stack radius, “ b ”, are most sensitive to the stability class. In our model, both the boundary-layer stability and the wind speed are used to calculate the rate of expansion of the plume. This dependence of expansion on the two variables explains the large dependence of “ a ” on the stability class (e.g. under unstable conditions the plume expands quickly regardless of wind speed and thus has a lower dependence on the wind speed). The plume volume expands super-linearly; as the volume of the plume increases, the rate of volume expansion also increases. The acceleration of the plume volume expansion is more pronounced under more unstable conditions, and the plume volume expansion rate is nearly constant under extremely stable conditions. As the stack radius determines the initial volume of the plume, it also determines in part the initial expansion rate of the plume, but this effect is more pronounced under more unstable conditions. The “ b ” exponent is therefore larger in magnitude for the more unstable stability classes. The exponents for variables that do not affect the expansion of the plume, such as D_p and σ , do not vary much for different stability classes.

Figure 3 shows the agreement in the fraction of particles remaining, F , between the fit parameterization and full multi-shelled Gaussian plume model for all stability classes. The fit tends to overestimate F for some cases for both high and low values of F , and the overestimations are larger for more unstable stability classes. However, we note that marine stratocumulus clouds, which would be targeted with this method, are unlikely to form under unstable conditions. Overall, the agreement of the parameterization with the full multi-shelled Gaussian plume model is good with root-mean-squared errors in F below 0.05 for all stability classes (as low as 0.01 for the most stable case) and correlation coefficients above 0.964 for all stability classes (as high as 0.999 for

Parameterization and global implications

G. S. Stuart et al.

[Title Page](#)[Abstract](#)[Introduction](#)[Conclusions](#)[References](#)[Tables](#)[Figures](#)[◀](#)[▶](#)[◀](#)[▶](#)[Back](#)[Close](#)[Full Screen / Esc](#)[Printer-friendly Version](#)[Interactive Discussion](#)

the most stable case). These results justify the semi-empirical equation that we use for the parameterization based on Turco and Yu (1997).

Figure 4 shows the dependence of F on each of the varied parameters. For each panel, one parameter is varied on the x-axis while the other four parameters are held fixed at their base-case values (Table 1). Each stability class is shown by the different colors, the full multi-shelled Gaussian plume model results are shown by the solid lines, and the fit parameterization is shown by the dashed lines. Panel 4a shows the results for varied wind speed. Increasing the wind speed greatly increases F because the initial particle concentrations are lower (air spends less time passing over the stack) and the plume expands more quickly with time. As with all panels, the most stable cases show the lowest F (plume expands the most slowly). In panel 4b, F increases somewhat with the stack radius. A wider stack radius leads to lower initial particle concentrations for the same particle emission rate. Panel 4c shows the sensitivity to the number of particles emitted. Because coagulation goes with the square of particle number concentration, F is strongly sensitive to the particle emissions rates and varies from over 0.8 to under 0.1 for the ranges tested. Panels 4d and 4e show that F is not strongly sensitive to the initial particle diameter or width of the distribution, but show a slight increase in F with increasing diameter (due to a reduction in the self-coagulation kernel across accumulation-mode sizes, Seinfeld and Pandis, 2006) and a slight decrease in F with increasing σ (due to broader particle size distributions coagulating more quickly, Seinfeld and Pandis, 2006).

There were several limitations of our modeling work discussed earlier. These involve an overestimation of particle size due to instant evaporation to 80 % RH equilibrium, an underestimation of the mixing due to turbulence generated by the initial upward motion of the sea-spray plume leaving the stack and vortex shedding due to the flow of air around the solid stack, an overestimation of the mixing under turbulent conditions due to the Gaussian-plume assumption, as well as the reflection of the plume from the ocean surface. F was not strongly sensitive to particle size (the difference between 200 nm and 400 nm particles was on the order of 0.05 or less), so we expect these

Parameterization and global implications

G. S. Stuart et al.

Title Page

Abstract

Introduction

Conclusions

References

Tables

Figures

◀

▶

◀

▶

Back

Close

Full Screen / Esc

Printer-friendly Version

Interactive Discussion



**Parameterization and
global implications**

G. S. Stuart et al.

Title Page

Abstract

Introduction

Conclusions

References

Tables

Figures

◀

▶

◀

▶

Back

Close

Full Screen / Esc

Printer-friendly Version

Interactive Discussion



to be the maximum errors due to the assumption of the particles instantly reaching their equilibrium size. Overall the underestimation of mixing due to the initial upward velocity of the particles and vortex-shedding would lead to somewhat larger values of F than predicted here (perhaps resembling lower stability classes). Jenkins and Forster (2013) found that including water with the emitted aerosols (as may occur during implementation) led to evaporation and reduced buoyancy within the plume. This caused a reduced vertical plume height but increased horizontal dispersion. As such, the particle concentrations within the plume were not significantly affected, suggesting that this effect would not significantly alter F . The importance of the reduced buoyancy on the subsequent transport of aerosols to the cloud is outside of the scope of the current work, and further investigation is planned. Regarding the overestimation of mixing under turbulent, unstable conditions, the marine boundary layer generally does not have strong instabilities, so this issue is likely minor. Regarding the ignoring of the ocean surface in the plume expansion, F decreases most quickly close to the emissions source. Generally, over 80 % of the coagulation occurs in the first 10 s. The time required for the plume to expand to the ocean surface will depend on the emissions height and the stability, but for the emissions heights of 20 m given in Salter et al. (2008) and neutral stability, the lower edge of the one-standard-deviation shell takes about 50 s to reach the ocean surface. We therefore expect that ignoring the ocean surface will not result significant errors in F under typical marine conditions.

Many cloud and large-eddy simulation models are able to resolve timesteps shorter than the time required for the fraction of particles remaining to asymptote to a constant value, and it therefore may seem counter-intuitive to use a parameterization that accounts for 50 min of aerosol processing. However, the parameterization is intended to account for the aerosol processing that occurs as the plume dilutes to the size of the model grid cell. So long as the spatial resolution of the cloud or large-eddy simulation is sufficiently coarse that F would asymptote before the plume dilutes to the spatial scale of the model, the temporal resolution of the model should not greatly affect the predicted value of F , even if it is less than the time required for the plume to dilute to

the spatial scale of the model. If the model has a finer spatial resolution, then F may be underestimated if the parameterization is used (both the parameterization and the resolved coagulation in the plume would each reduce F).

6 Global model experiment design and results

In order to assess the effect of the parameterization on predictions of marine cloud brightening efficacy, we did three 5 yr global simulations using the ECHAM-HAMMOZ model (Sect. 2.3) with an additional 1 yr spin-up period. The model was run with horizontal resolution T63 (corresponding roughly to $1.9^\circ \times 1.9^\circ$ grid), 31 vertical layers extending to 10 hPa, and prescribed climatological sea surface temperatures.

In the control run (ctrl) there was no geoengineering applied. The reference geoengineering simulations (geo-ref) had artificial sea salt injections applied in three stratocumulus regions (indicated by the red lines in Fig. 5) that had been previously assessed as optimal to maximize the radiative effect from geoengineering (Partanen et al., 2012). The injected sea-salt particle number flux F_n with 10 m wind speed of u was set according to the formula:

$$F = \begin{cases} 3.1 \times 10^5 \times \left(\frac{u}{1 \text{ m s}^{-1}}\right)^{1.5} \text{ m}^{-2} \text{ s}^{-1}, & u < 7 \text{ m s}^{-1} \\ 3.1 \times 10^5 \times 7^{1.5} \text{ m}^{-2} \text{ s}^{-1}, & u \geq 7 \text{ m s}^{-1} \end{cases} \quad (6)$$

The mass flux (about 20.6 Tgyr^{-1}) and the functional form of injection and were identical to the simulation GEO described by Partanen et al. (2012), although the number flux was different due to the different particle size. The mass-mean diameter of the injected particles was set to 200 nm, which, with a mode standard deviation of 1.59, corresponds to a number-median diameter of 145 nm used as input for the parameterization.

The other geoengineering simulation (geo-coag) was identical to geo-ref except that the injected sea-salt number flux and number-median diameter were modified by the

Title Page

Abstract

Introduction

Conclusions

References

Tables

Figures

◀

▶

◀

▶

Back

Close

Full Screen / Esc

Printer-friendly Version

Interactive Discussion



Parameterization and
global implications

G. S. Stuart et al.

Title Page

Abstract

Introduction

Conclusions

References

Tables

Figures

◀

▶

◀

▶

Back

Close

Full Screen / Esc

Printer-friendly Version

Interactive Discussion



sub-grid coagulation parameterization. We assumed neutral atmospheric stability for all geoengineered regions during the simulation and a stack radius of 1.2 m. The input number flux to the parameterization used the same wind speed dependence as Eq. (6), and was set to $1.2 \times 10^{17} \text{ s}^{-1}$ (corresponding to sea water flux of 30 kg s^{-1} , see Sects. 2.2 and 3) at wind speeds greater than or equal to 7 m s^{-1} . As we assumed always neutral atmospheric stability and a fixed size distribution of emitted particles as inputs to the parameterization, the final number and particle diameter after the parameterization depended only on wind speed.

The number flux of injected sea-salt particles was on average 61 % lower and particle number-median diameter was 40 % higher in geo-coag than in geo-ref. There was substantial spatial and temporal variation as the fraction of remaining particles varied between about 20 % and 60 % (not shown in a figure).

The lower number emissions in geo-coag lead to a notable decrease in cloud droplet number concentration (CDNC). We diagnosed the cloud-top CDNC by calculating the mean value of CDNC in the highest lying grid cell with warm clouds for each time step and grid-cell with positive cloud cover. Figure 5a shows the relative difference of cloud-top CDNC between geo-coag and geo-ref. In the North Pacific region, the 5 yr-mean cloud-top CDNC was as much as 56 % lower in geo-coag than in geo-ref. Averaging over all the emission regions, the mean change was -46% . Regional mean values of cloud-top CDNC for the geoengineered regions are given in Table 3. The highest mean CDNC was achieved in geo-ref in the South Atlantic region (754 cm^{-3}). The corresponding value in geo-coag was 42 % lower.

The lower number of aerosol particles and cloud droplets also caused differences in the radiative response. We evaluated the total aerosol radiative effect (both direct and indirect effects) as radiative flux perturbation (RFP) (Haywood et al., 2009), i.e., difference in net total (shortwave and longwave) radiation at the top of the atmosphere between the geoengineering runs and the control simulation. The global mean RFPs (with respect to ctrl) in geo-ref and geo-coag were -1.5 W m^{-2} and -0.8 W m^{-2} respec-

**Parameterization and
global implications**

G. S. Stuart et al.

Title Page

Abstract

Introduction

Conclusions

References

Tables

Figures

◀

▶

◀

▶

Back

Close

Full Screen / Esc

Printer-friendly Version

Interactive Discussion



We have fit our results to a parameterization that depends on the six parameters using a semi-empirical formula based on Turco and Yu (1997). The parameterization has a mean-squared error in the fraction of particles remaining of 0.05 for very unstable conditions and 0.01 for stable conditions, and the correlation coefficients range from 0.964 for very unstable conditions to 0.999 for stable conditions. We provide Fortran code of this parameterization as Supplement that calculates both the fraction of particles remaining and the final number-median diameter of the distribution.

We have implemented this parameterization into a global-scale aerosol-climate model, and we found that accounting for this sub-grid-scale coagulation reduced the number flux of injected particles by 61 %, resulting in reductions in CDNC and RFP over source regions of about 46 % and 25 %, respectively. The global mean RFP was reduced by 47 %.

Previous cloud-resolving and global-scale modeling studies are unable to resolve in-plume coagulation due to coarse spatial resolution. The results of this work show that such studies will overestimate the number of injected particles that reach cloud base. Using the parameterization developed in this paper, future studies will be able to account for these effects.

Acknowledgements. We gratefully acknowledge NSERC and the Academy of Finland (projects 140867 and 250348) for funding support and ACEnet for computational support. The ECHAM-HAMMOZ model is developed by a consortium composed of ETH Zurich, Max Planck Institut für Meteorologie, Forschungszentrum Jülich, University of Oxford, and the Finnish Meteorological Institute and managed by the Center for Climate Systems Modeling (C2SM) at ETH Zurich.

References

- Abdul-Razzak, H. and Ghan, S. J.: A parameterization of aerosol activation: 2. multiple aerosol types, *J. Geophys. Res.*, 105, 6837–6844, doi:10.1029/1999JD901161, 2000.
- Albrecht, B.: Aerosols, cloud microphysics, and fractional cloudiness, *Science*, 245, 1227–1230, 1989.

Parameterization and
global implications

G. S. Stuart et al.

Title Page

Abstract

Introduction

Conclusions

References

Tables

Figures

◀

▶

◀

▶

Back

Close

Full Screen / Esc

Printer-friendly Version

Interactive Discussion



Alterskjær, K. and Kristjánsson, J. E.: The sign of the radiative forcing from marine cloud brightening depends on both particle size and injection amount, *Geophys. Res. Lett.*, 40, 210–215, doi:10.1029/2012gl054286, 2013.

Alterskjær, K., Kristjánsson, J. E., and Seland, Ø.: Sensitivity to deliberate sea salt seeding of marine clouds – observations and model simulations, *Atmos. Chem. Phys.*, 12, 2795–2807, doi:10.5194/acp-12-2795-2012, 2012.

Bala, G., Caldeira, K., Nemani, R., Cao, L., Ban-Weiss, G., and Shin, H.-J.: Albedo enhancement of marine clouds to counteract global warming: impacts on the hydrological cycle, *Clim. Dynam.*, 37, 915–931, doi:10.1007/s00382-010-0868-1, 2011.

Bower, K., Choulaton, T., Latham, J., Sahraei, J., and Salter, S.: Computational assessment of a proposed technique for global warming mitigation via albedo-enhancement of marine stratocumulus clouds, *Atmos. Res.*, 82, 328–336, doi:10.1006/Asle.2002.0048, 2006.

Dentener, F., Kinne, S., Bond, T., Boucher, O., Cofala, J., Generoso, S., Ginoux, P., Gong, S., Hoelzemann, J. J., Ito, A., Marelli, L., Penner, J. E., Putaud, J.-P., Textor, C., Schulz, M., van der Werf, G. R., and Wilson, J.: Emissions of primary aerosol and precursor gases in the years 2000 and 1750 prescribed data-sets for AeroCom, *Atmos. Chem. Phys.*, 6, 4321–4344, doi:10.5194/acp-6-4321-2006, 2006.

Fast, J. D., Gustafson Jr., W. I., Easter, R. C., Zaveri, R. A., Barnard, J. C., Chapman, E. G., Grell, G. A., and Peckham, S. E.: Evolution of ozone, particulates, and aerosol direct radiative forcing in the vicinity of Houston using a fully coupled meteorology-chemistry-aerosol model, *J. Geophys. Res.*, 111, D21305, doi:10.1029/2005jd006721, 2006.

Forster, P., Ramaswamy, V., Artaxo, P., Berntsen, T., Betts, R., Fahey, D. W., Haywood, J., Lean, J., Lowe, D. C., Myhre, G., Nganga, J., Prinn, R., Raga, G., Schulz, M., and Dorland, R. V.: Changes in atmospheric constituents and in radiative forcing, in: *Climate Change 2007: The Physical Science Basis, Contribution of Working Group I to the Fourth Assessment Report of the Intergovernmental Panel on Climate Change*, edited by: Miller, H. L., Cambridge University Press, Cambridge, UK and New York, NY, USA, 129–234, 2007.

Fuchs, N. A.: *Mechanics of Aerosols*, Pergamon, New York, 1964.

Haywood, J., Donner, L., Jones, A., and Golaz, J.-C.: Global indirect radiative forcing caused by aerosols: IPCC (2007) and beyond, in: *Clouds in the Perturbed Climate System: Their Relationship to Energy Balance, Atmospheric Dynamics, and Precipitation*, edited by: Heintzenberg, J. and Charlson, R. J., Strüngmann Forum Report, MIT Press, Cambridge, 451–467, 2009.

Parameterization and
global implications

G. S. Stuart et al.

Title Page

Abstract

Introduction

Conclusions

References

Tables

Figures

◀

▶

◀

▶

Back

Close

Full Screen / Esc

Printer-friendly Version

Interactive Discussion



Heintzenberg, J., Covert, D. C., and Van Dingenen, R.: Size distribution and chemical composition of marine aerosols: a compilation and review, *Tellus B*, 52, 1104–1122, doi:10.3402/tellusb.v52i4.17090, 2000.

Hudischewskij, A. B. and Seigneur, C.: Mathematical modeling of the chemistry and physics of aerosols in plumes, *Environ. Sci. Technol.*, 23, 413–421, doi:10.1021/es00181a005, 1989.

Jenkins, A. K. L. and Forster, P. M.: The inclusion of water with the injected aerosol reduces the simulated effectiveness of marine cloud brightening, *Atmos. Sci. Lett.*, accepted, 2013.

Jenkins, A. K. L., Forster, P. M., and Jackson, L. S.: The effects of timing and rate of marine cloud brightening aerosol injection on albedo changes during the diurnal cycle of marine stratocumulus clouds, *Atmos. Chem. Phys.*, 13, 1659–1673, doi:10.5194/acp-13-1659-2013, 2013.

Jones, A., Haywood, J., and Boucher, O.: Climate impacts of geoengineering marine stratocumulus clouds, *J. Geophys. Res.*, 114, D10106, doi:10.1029/2008JD011450, 2009.

Klug, W.: A method for determining diffusion conditions from synoptic observations, *Staub Reinhalt. Luft*, 29, 14–20, 1969.

Korhonen, H., Carslaw, K. S., and Romakkaniemi, S.: Enhancement of marine cloud albedo via controlled sea spray injections: a global model study of the influence of emission rates, microphysics and transport, *Atmos. Chem. Phys.*, 10, 4133–4143, doi:10.5194/acp-10-4133-2010, 2010.

Latham, J.: Control of global warming?, *Nature*, 347, 339–340, 1990.

Latham, J., Bower, K., Choulaton, T., Coe, H., Connolly, P., Cooper, G., Craft, T., Foster, J., Gadian, A., Galbraith, L., Iacovides, H., Johnston, D., Launder, B., Leslie, B., Meyer, J., Neukermans, A., Ormond, B., Parkes, B., Rasch, P., Rush, J., Salter, S., Stevenson, T., Wang, H., Wang Q., and Wood, R.: Marine cloud brightening, *Philos. Trans. A*, 370, 4217–62, doi:10.1098/rsta.2012.0086, 2012.

Lazaridis, M., Isukapalli, S. S., and Georgopoulos, P. G.: Modelling of aerosol processes in plumes, *Tellus B*, 53, 83–93, doi:10.1034/j.1600-0889.2001.01165.x, 2001.

Lewis, E. R. and Schwartz, S. E.: Sea Salt Aerosol Production: Mechanisms, Methods, Measurements and Models: a Critical Review, American Geophysical Union, Washington DC, 2004.

Lohmann, U., Stier, P., Hoose, C., Ferrachat, S., Kloster, S., Roeckner, E. and Zhang, J.: Cloud microphysics and aerosol indirect effects in the global climate model ECHAM5-HAM, *Atmos. Chem. Phys.*, 7, 3425–3446, doi:10.5194/acp-7-3425-2007, 2007.

Parameterization and
global implications

G. S. Stuart et al.

Title Page

Abstract

Introduction

Conclusions

References

Tables

Figures

◀

▶

◀

▶

Back

Close

Full Screen / Esc

Printer-friendly Version

Interactive Discussion



McKay, M., Beckman, R., and Conover, W.: A comparison of three methods for selecting values of input variables in the analysis of output from a computer code, *Technometrics*, 29, 239–245, 1979.

Lohmann, U. and Hoose, C.: Sensitivity studies of different aerosol indirect effects in mixed-phase clouds, *Atmos. Chem. Phys.*, 9, 8917–8934, doi:10.5194/acp-9-8917-2009, 2009.

Lohman, K., Seigneur, C., Edgerton, E., and Jansen, J.: Modeling mercury in power plant plumes., *Environ. Sci. Technol.*, 40, 3848–54, 2006.

Partanen, A.-I., Kokkola, H., Romakkaniemi, S., Kerminen, V.-M., Lehtinen, K. E. J., Bergman, T., Arola, A., and Korhonen, H.: Direct and indirect effects of sea spray geoengineering and the role of injected particle size, *J. Geophys. Res.*, 117, D02203, doi:10.1029/2011JD016428, 2012.

Pasquill, F.: The estimation of the dispersion of windborne material, *Meteorol. Mag.*, 90, 33–49, 1961.

Pringle, K. J., Carslaw, K. S., Fan, T., Mann, G.W., Hill, A., Stier, P., Zhang, K., and Tost, H.: A multi-model assessment of the impact of sea spray geoengineering on cloud droplet number, *Atmos. Chem. Phys.*, 12, 11647–11663, doi:10.5194/acp-12-11647-2012, 2012.

Rasch, P. J., Latham, J., and Chen, C.-C.: Geoengineering by cloud seeding: influence on sea ice and climate system, *Environ. Res. Lett.*, 4, 045112, doi:10.1088/1748-9326/4/4/045112, 2009.

Rosa, E. A. and Dietz, T.: Human drivers of national greenhouse-gas emissions, *Nature Clim. Change*, 2, 581–586, 2012.

The Royal Society: *Geoengineering the Climate, Science, Governance and Uncertainty*, The Royal Society, London, 2009.

Salter, S., Sortino, G., and Latham, J.: Sea-going hardware for the cloud albedo method of reversing global warming., *Philos. Trans. A*, 366, 3989–4006, doi:10.1098/rsta.2008.0136, 2008.

Seigneur, C., Wu, X., Constantinou, E., Gillespie, P., Bergstrom, R. W., Sykes, I., Venkatram, A., and Karamchandani, P.: Formulation of a second-generation reactive plume and visibility model, *J. Air Waste Manage. Assoc.*, 47, 176–184, 1997.

Seinfeld, J. H. and Pandis, S. N.: *Atmospheric Chemistry Physics: From Air Pollution to Climate Change*, 2nd edn., John Wiley and Sons, Inc., Hoboken, New Jersey, 2006.

Parameterization and
global implications

G. S. Stuart et al.

Title Page

Abstract

Introduction

Conclusions

References

Tables

Figures

◀

▶

◀

▶

Back

Close

Full Screen / Esc

Printer-friendly Version

Interactive Discussion



Skamarock, W. C., Klemp, J. B., Dudhia, J., Gill, D. O., Barker, D. M., Duda, M. G., Huang, X.-Y., Wang, W., and Powers, J. G.: A Description of the Advanced Research WRF Version 3, NCAR Technical Note, NCAR/TN-475+STR, 2008.

Stevens, R. G., Pierce, J. R., Brock, C. A., Reed, M. K., Crawford, J. H., Holloway, J. S., Ryerson, T. B., Huey, L. G., and Nowak, J. B.: Nucleation and growth of sulfate aerosol in coal-fired power plant plumes: sensitivity to background aerosol and meteorology, *Atmos. Chem. Phys.*, 12, 189–206, doi:10.5194/acp-12-189-2012, 2012.

Stier, P., Feichter, J. and Kinne, S.: The aerosol-climate model ECHAM5-HAM, *Atmos. Chem. and Phys.*, 5, 1125–1156, doi:10.5194/acp-5-1125-2005, 2005.

Tu, C.-X. and Liu, S.: Nanoparticle coagulation and dispersion in a turbulent planar jet with constraints, *Therm. Sci.*, 16, 1497–1501, 2012.

Turco, R. and Yu, F.: Aerosol invariance in expanding coagulating plumes, *Geophys. Res. Lett.*, 24, 1223–1226, 1997.

Twomey, S.: Pollution and planetary albedo, *Atmos. Environ.*, 8, 1251–1256, doi:10.1016/0004-6981(74)90004-3, 1974.

Vignati, E., Wilson, J., and Stier, P.: M7: An efficient size-resolved aerosol microphysics module for large-scale aerosol transport models, *J. Geophys. Res.*, 109, D22202, doi:10.1029/2003JD004485, 2004.

Wang, H., Skamarock, W. C., and Feingold, G.: Evaluation of scalar advection schemes in the advanced research WRF model using large-Eddy simulations of aerosol–cloud interactions, *Mon. Weather Rev.*, 137, 2547–2558, doi:10.1175/2009MWR2820.1, 2009.

Wang, H., Rasch, P. J., and Feingold, G.: Manipulating marine stratocumulus cloud amount and albedo: a process-modelling study of aerosol-cloud-precipitation interactions in response to injection of cloud condensation nuclei, *Atmos. Chem. Phys.*, 11, 4237–4249, doi:10.5194/acp-11-4237-2011, 2011.

Wen, F., Kamalu, N., Chung, J., Crowe, C., and Troutt, T.: Particle Dispersion by Vortex Structures in Plane Mixing Layers, *J. Fluids Eng.*, 114, 657–666, doi:10.1115/1.2910082, 1992.

Zaveri, R. A. and Peters, L. K.: A new lumped structure photochemical mechanism for large-scale applications, *J. Geophys. Res.*, 104, 30387–30415, doi:10.1029/1999jd900876, 1999.

Zaveri, R. A., Easter, R. C., Fast, J. D., and Peters, L. K.: Model for simulating aerosol interactions and chemistry (MOSAIC), *J. Geophys. Res.*, 113, D13204, doi:10.1029/2007jd008782, 2008.

Zhang, K., O'Donnell, D., Kazil, J., Stier, P., Kinne, S., Lohmann, U., Ferrachat, S., Croft, B., Quaas, J., Wan, H., Rast, S., and Feichter, J.: The global aerosol-climate model ECHAM-HAM, version 2: sensitivity to improvements in process representations, *Atmos. Chem. Phys.*, 12, 8911–8949, doi:10.5194/acp-12-8911-2012, 2012.

Parameterization and global implications

G. S. Stuart et al.

Title Page

Abstract

Introduction

Conclusions

References

Tables

Figures



Back

Close

Full Screen / Esc

Printer-friendly Version

Interactive Discussion



Parameterization and
global implications

G. S. Stuart et al.

Title Page

Abstract

Introduction

Conclusions

References

Tables

Figures

◀

▶

◀

▶

Back

Close

Full Screen / Esc

Printer-friendly Version

Interactive Discussion

**Table 1.** The variables explored in the plume modelling and the range of values used for each.

Variable	Minimum	Base Case	Maximum
Wind speed (v_w)	4 ms^{-1}	8 ms^{-1}	20 ms^{-1}
Particle number emission rate (P)	$1.1 \times 10^{16} \text{ s}^{-1}$	$1.1 \times 10^{17} \text{ s}^{-1}$	$1.1 \times 10^{18} \text{ s}^{-1}$
Number-median dry diameter (D_p)	100 nm	200 nm	400 nm
Geometric standard deviation (σ)	1 (monodisperse)	1.2	2
Emission-source radius (R_s)	0.6 m	1.2 m	2.4 m

Parameterization and
global implications

G. S. Stuart et al.

Table 2. The fitted exponents and constant corresponding to Eq. (5) for each stability class as well as the root-mean-square error and correlation coefficient in the fraction of particles remaining associated with each fit. The exponents a , b , c , d , and e correspond to the parameters v_w , R_s , P , σ , and D_p , respectively. Stability classes: A, extremely unstable; B, moderately unstable; C, slightly unstable; D, neutral; E, slightly stable; and F, moderately stable.

Stability Class	a	b	c	d	e	k	Root-mean-square error	Correlation coefficient
A	-0.84	-0.40	0.51	0.30	-0.13	1.282	0.046	0.9646
B	-0.96	-0.39	0.56	0.33	-0.14	1.219	0.041	0.9761
C	-1.17	-0.36	0.65	0.37	-0.16	0.969	0.030	0.9905
D	-1.28	-0.30	0.69	0.38	-0.17	0.774	0.023	0.9951
E	-1.34	-0.23	0.72	0.38	-0.18	0.611	0.018	0.9971
F	-1.41	-0.13	0.76	0.37	-0.18	0.363	0.010	0.9990

Title Page

Abstract

Introduction

Conclusions

References

Tables

Figures

◀

▶

◀

▶

Back

Close

Full Screen / Esc

Printer-friendly Version

Interactive Discussion



Parameterization and
global implications

G. S. Stuart et al.

Title Page

Abstract

Introduction

Conclusions

References

Tables

Figures

I◀

▶I

◀

▶

Back

Close

Full Screen / Esc

Printer-friendly Version

Interactive Discussion



Table 3. Mean cloud-top cloud droplet number concentration (cm^{-3}) averaged over cloudy time-steps for the geoengineered regions in North Pacific (NP), South Pacific (SP), and South Atlantic (SA) as shown in Fig. 5.

Simulation	NP	SP	SA
ctrl	103	131	166
geo-ref	607	624	754
geo-coag	302	345	436

Parameterization and
global implications

G. S. Stuart et al.

Title Page

Abstract

Introduction

Conclusions

References

Tables

Figures

I◀

▶I

◀

▶

Back

Close

Full Screen / Esc

Printer-friendly Version

Interactive Discussion



Table 4. Mean radiative flux perturbation (Wm^{-2}) for the geoengineered regions in North Pacific (NP), South Pacific (SP), and South Atlantic (SA) as shown in Fig. 5. The last column is the global mean value (GM).

Simulation	NP	SP	SA	GM
geo-ref	−31.1	−30.4	−29.2	−1.5
geo-coag	−21.8	−24.4	−23.8	−0.8

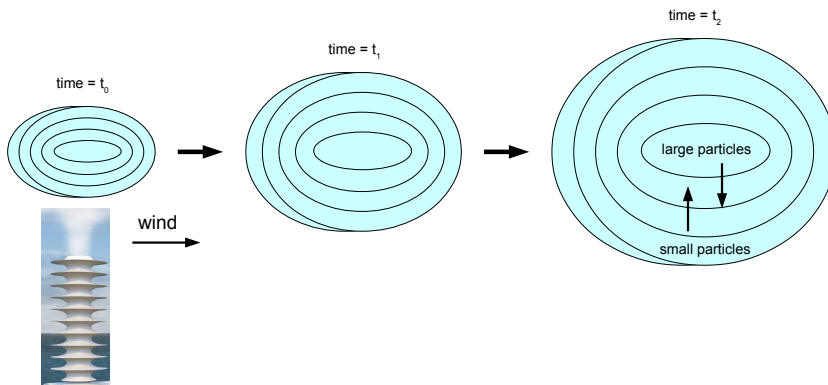


Fig. 1. Schematic of the Gaussian plume model. The shells expand with time due to dilution. Coagulation proceeds more quickly in the inner shells, due to higher particle concentrations and thus there is a net flux of small particles to the inner shells and large particles to the outer shells.

Title Page	
Abstract	Introduction
Conclusions	References
Tables	Figures
◀	▶
◀	▶
Back	Close
Full Screen / Esc	
Printer-friendly Version	
Interactive Discussion	



Parameterization and
global implications

G. S. Stuart et al.

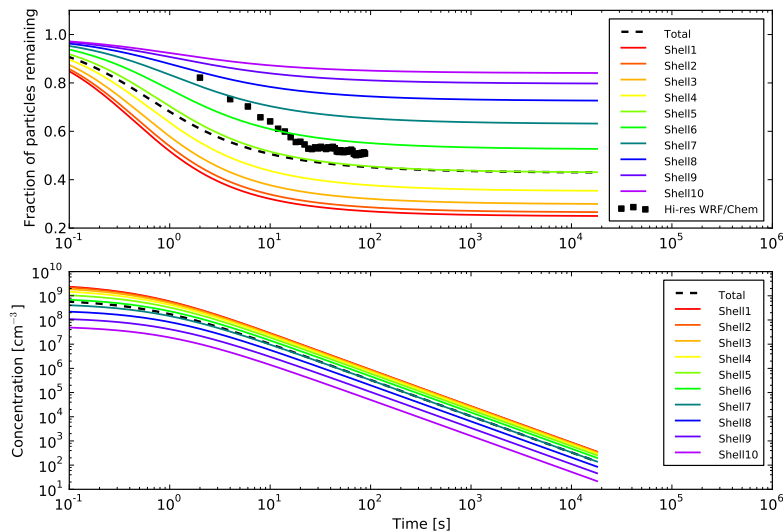


Fig. 2. The fraction of particles remaining and the concentrations are shown over time for each shell for the base case. The black dashed line shows the average across the plume, and the black square points show high resolution results from the WRF/Chem large-eddy simulation model.

[Title Page](#)[Abstract](#)[Introduction](#)[Conclusions](#)[References](#)[Tables](#)[Figures](#)[◀](#)[▶](#)[◀](#)[▶](#)[Back](#)[Close](#)[Full Screen / Esc](#)[Printer-friendly Version](#)[Interactive Discussion](#)

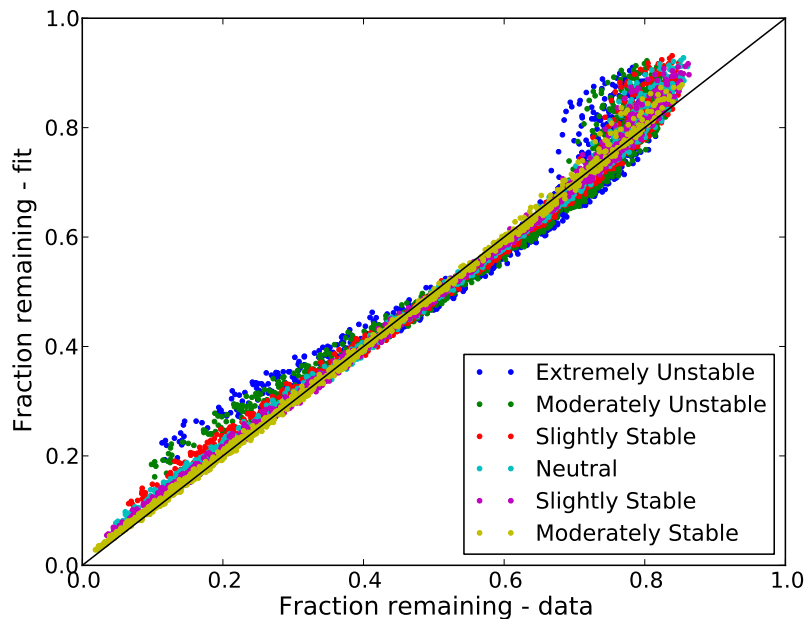


Fig. 3. The fraction of particles remaining for the parameterization (fit) compared to full Gaussian multi-shelled model results (data). The black line represents a perfect match between the fit and model.

Parameterization and global implications

G. S. Stuart et al.

Title Page	
Abstract	Introduction
Conclusions	References
Tables	Figures
◀	▶
◀	▶
Back	Close
Full Screen / Esc	
Printer-friendly Version	
Interactive Discussion	



Parameterization and
global implications

G. S. Stuart et al.

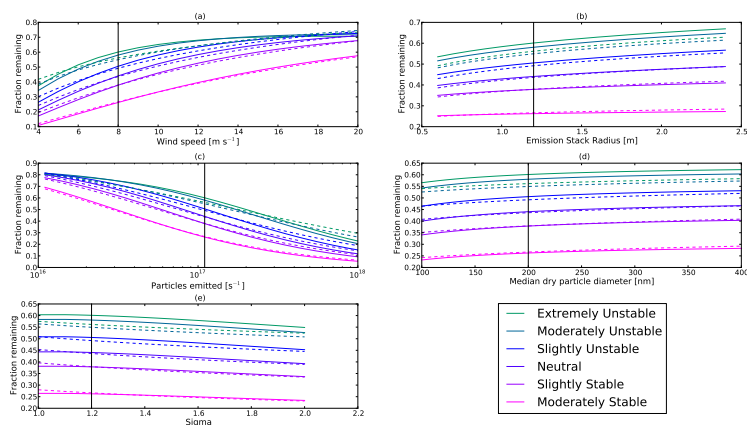


Fig. 4. The dependence of F on each of the varied parameters for all stability classes. In each plot, one parameter is varied while the other four are kept at their base-case values. The full multi-shelled Gaussian plume model results are shown by the solid lines, and the fit parameterization is shown by the dashed lines. The solid black vertical lines indicate the base-case value for each parameter.

Title Page

Abstract

Introduction

Conclusions

References

Tables

Figures



Back

Close

Full Screen / Esc

Printer-friendly Version

Interactive Discussion



Parameterization and
global implications

G. S. Stuart et al.

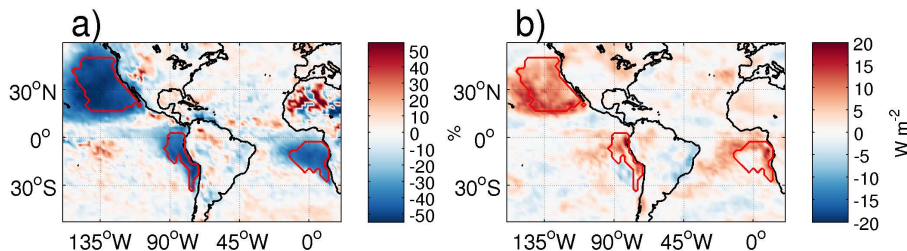


Fig. 5. (a) The relative difference in 5 yr mean cloud-top cloud droplet number concentration between simulations geo-coag and geo-ref. (b) 5 yr mean radiative flux perturbation between simulations geo-coag and geo-ref. Red values mean larger values in the geo-coag simulation.

Title Page

Abstract

Introduction

Conclusions

References

Tables

Figures

◀

▶

◀

▶

Back

Close

Full Screen / Esc

Printer-friendly Version

Interactive Discussion

